JOURNAL OF MATERIALS SCIENCE **36** (2001) 5839–5844

Preparation of samaria-doped ceria for solid-oxide fuel cell electrolyte by a modified sol-gel method

G. B. JUNG, T. J. HUANG*
Department of Chemical Engineering, National Tsing Hua University, Hsinchu, Taiwan, ROC

M. H. HUANG
Department of Chemical Engineering, National Kaohsiung Institute of Technology, Kaohsiung, Taiwan, ROC

C. L. CHANG
Industrial Technology Research Institute, Hsinchu, Taiwan, ROC

Samaria-doped ceria powders were prepared by the sol-gel method with different processes. The characteristics of the sample were investigated by particle size distribution, X-ray diffraction, crystallite size, and density analyses. A modified process of the sol-gel method was proposed in this work. It involves treating the gel with high-carbon (long chain, high boiling point) alcohol. It yields near-completely soft-agglomerated nanocrystalline powders which are easily sintered in air to yield near-fully relative density at 1300°C, which is significantly lower than temperatures of 1400–1500°C required by the doped-ceria powder prepared via the previous processes of the sol-gel method.

1. Introduction

Doped ceria has been investigated over past 20 years as an oxide-ion electrolyte possibly competitive with stabilized zirconia for use in a solid-oxide fuel cell (SOFC) [1–3]. Advantage of using ceria-based electrolytes is well known as higher ionic conductivity. Thus, it is expected, with a similar power output, to lower the operation temperature for SOFC stacks from 900–1000°C currently for zirconia-based cells to 700–800°C for ceria-based cells. This advantage makes the fuel cell using ceria-based electrolyte competitive with other types of fuel cells operating at lower temperature [4–6]. In addition, the reduction in operation temperature would avoid high temperature interaction and inter-diffusion that take place between cell components and thus increase the stack lifetime. It also relieves materials constraints and allows more flexibility in regard to the choice of stack materials (e.g., the use of metallic rather than ceramic separators) and thus lowers the fabrication costs.

Disadvantages related to the use of the ceria material but not to the case of zirconia must be addressed. These include easy reducibility in the fuel-gas environment [7], which shorts the cell and results in the power loss. The disadvantage of the reducibility can be avoided, for example, by coating the mixed conductive ceria material with a thin protective layer of purely ionic conductive zirconia, thereby blocking the electronic leak current. This has been demonstrated for cheaper and more-practical method such as tape casting.

Ceria diffusion is important above 1400°C. Thus, an important requirement for the cofiring feasibility of double-layered tape-cast thick ceria with zirconia is the densification of ceria at normal temperature (<1400°C) in order to prevent the chemical interaction between these two components at high temperature. However, doped ceria has been found to be difficult to sinter at temperature required for SOFC fabrication to nearfull density ceramics by a number of workers, even at elevated temperatures (>1500°C). Table I presents a selection of the results. Inspection of the literatures reveals that it's difficult to obtain a dense doped-ceria ceramic by conventional ceramic techniques at sintering temperatures $T_s = 1700$°C in air [8].

The gel precipitation process allows the production of mixed oxides of high homogeneity. By the sol-gel method, single phases can be achieved at low temperatures and nano-crystalline particles can be easily obtained [5]. Although ultrafine powders prepared by the sol-gel method allows sintering of the samples into highly dense ceramic pellets at significantly low temperature of 1400°C have been published [13], the precipitation of the materials must be controlled by addition of nitric acid at carefully controlled $[H^+]$:[Ce(IV)] mole ratio to yield a stable sol solution at pH ~3.3 and the transformation of the sol to gel is time-consuming (over a period of 2 days).

Readey *et al*. [15] found that the sintering behavior is very sensitive to the gel-dealing solvent because hard agglomerates form when the precipitated gels are

*Author to whom all correspondence should be addressed.

TABLE I Selected literatures on the synthesis of doped-ceria powder and its sintering behavior

Reference	Amount of doping (mole %)	Powder preparation method	Sintering temperature (degrees C) and time (h)	Relative density (%)
Reiss *et al*. [8]	18% $GdO_{1.5}$	Solid state	1700 (2)	95–98
Kudo *et al*. [9]	30% $YO_{1.5}$	Solid state	1800 (2–3)	96
Zhen *et al*. [10]	20% $YO_{1.5}$	Solid state	1600 (6)	94
Huang *et al*. [11]	10% $GdO_{1.5}$	Sol-gel	1585 (6)	99
Herle *et al*. [12]	20% $SmO_{1.5}$			
	20% $GdO_{1.5}$	Sol-gel	1300 (4)	97
	20% $YO_{1.5}$			
Huang *et al*. [13]	$SmO_{1.5}$	Sol-gel	1400 (10)	95
Dikmen *et al*. [14]	$LaO_{1.5}$	Sol-gel	1400 (4)	95–97

washed with water, whereas soft agglomerates form when they are washed with ethanol. However, in this study, we found that the powder characteristics of the ethanol-washed gel did not show much difference with those of the water-washed gel. Therefore, a modified process by treating the gel with high carbon (long chain, high boiling-point) alcohol of octanol during the preparation of the samaria-doped ceria (SDC) powders via the sol-gel method is investigated and compared with those treated with water and ethanol.

In this work, the modified process of the sol-gel method for the development of doped-ceria powders capable of sintering to full density below 1400°C, which is important to facilitate SOFC fabrication. The agglomerate structures of the gels produced from different processes are studied in order to understand how the reaction mechanisms result in different degree of agglomeration.

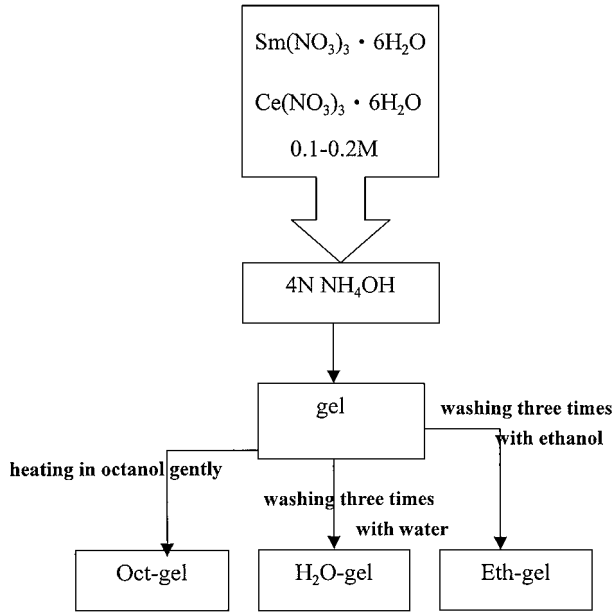

Figure 1 Flow chart of the sol-gel preparation.

2. Experiment details

2.1. Gel preparation

The 20 mole% samaria-doped ceria samples were prepared from reagent-grade (99% purity Aldrich Chemical Co.) metal nitrates of $Sm(NO_3)_3 \cdot 6H_2O$ and $Ce(NO_3)_3 \cdot 6H_2O$. The appropriate proportions of samarium nitrate and cerium nitrate were dissolved in distilled water to make 0.1–0.2 M solutions. Hydrolysis of the metal salts to hydroxides was obtained by dropping into NH_4OH solution. To eliminate the inhomogeneous gels, nitrate solutions were added dropwise to a 4N solution of NH_4OH and the solution was maintained at pH >10. A distinct precipitate gel was formed when the nitrate solution was dropped into the NH_4OH solution. The gel was easily isolated by vacuum filtered. The recovered gel was divided into three parts for further investigation (see the flow chart in Fig. 1).

The first part of the gel was washed with water three times. The gel obtained after washing with water was called H_2O-gel. The second part of the gel was washed with ethanol three times. The gel obtained after washing with ethanol was called Eth-gel. The third part of the gel was immersed in octanol, stirred by a magnetic stirrer and heated on a plate with very low power output. During the process of heating, octanol was added to the solution frequently to make sure that water within the gel will be completely replaced by octanol. The gel obtained from this process was called Oct-gel.

2.2. Thermal analysis

The three kinds of gels were dried at 80°C in a tubular dryer overnight. The dried H_2O-gel and Eth-gel were hard and glass-like while the dry Oct-gel was soft and friable. The dried gel was studied using a differential thermal analyzer (Stanton Redcraft Ltd., SDT-2960) in an oxidizing atmosphere (flow rate 150 ml/min). Weighed amounts of the dried gel (∼13 mg) and a reference material (Al_2O_3) were placed in cylindrical platinum crucibles and heated from 50 to 1000°C (30°C/min). The results of the differential thermal analysis (DTA) and thermogravimetric analysis (TG) as a function of temperature were plotted simultaneously.

2.3. X-ray analysis and crystallite size determination

X-ray diffraction (XRD) technique was used to determine the crystal structure and phase. The gels were heated at 80, 500 and 1200°C for 5 hours. X-ray spectra were obtained over the 2Θ range of 20°–80° at a speed of 10°/min by a Phillips diffractometer (PW1710) with Cu K_α radiation. The diffractometer was operated at 40 kV and 40 mA. The crystallite size can be determined for the dried gels by the well-known Scherrer relation.

2.4. Particle size analysis

Particle size analysis was performed on a Laser particle analyzer (LPA-3000) with He-Ne laser obtained from OTSUKA. The powders obtained from calcining the three kinds of gels at 500°C for 5 hours were called H_2O-powder, Eth-powder, and Oct-powder. The powders were first milled by ball miller and then dispersed in water and stirred by a magnetic stirrer for 20 minutes. This suspension was then added to the sample cell in order to obtain data for the particle size distribution.

2.5. Density determination

The powders were pressed to disk in air. Green compact disks of the H_2O-powder, Eth-powder, and Oct-powder samples were calcined at 1000, 1100, 1200, 1300, 1400°C in air for five hours with a heating rate of 5°C/min. The resultant sintered densities (D_{rs}) of the disks were determined by the Archimedes method,

$$D_{rs} = \frac{W_1 \rho}{W_2 - W_3} \tag{1}$$

where W_1 is the dry weight, W_2 is the wet weight (water in body), W_3 is the body's submerged weight without fine wire, and ρ is the density of the solvent(water). The theoretical density (D_{th}) and relative density could then be calculated by

$$D_{th} = \frac{4}{N_A \alpha^3}\left[(1-C)M_{Ce} + C M_{Sm} + \left(2 - \frac{1}{2}C\right)M_0\right] \tag{2}$$

$$\text{Relative density} = \frac{D_{rs}}{D_{th}} \tag{3}$$

with $C = 0.2$; where N_A is the Avogardro number and M refers to the atomic weight.

3. Results and discussion

3.1. Thermal analysis result

As shown in Fig. 2, the results of DTA in air consist of a small endothermic peak at around 100°C for both

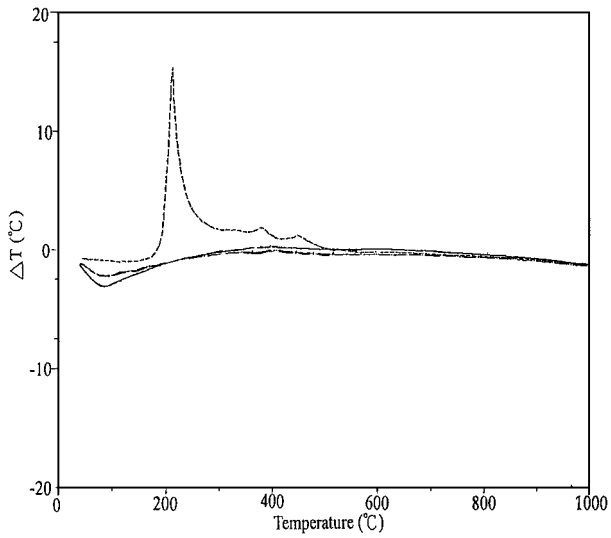

Figure 2 DTA results for H_2O-gel (solid line), Eth-gel (-.-.-), and Oct-gel (- - -).

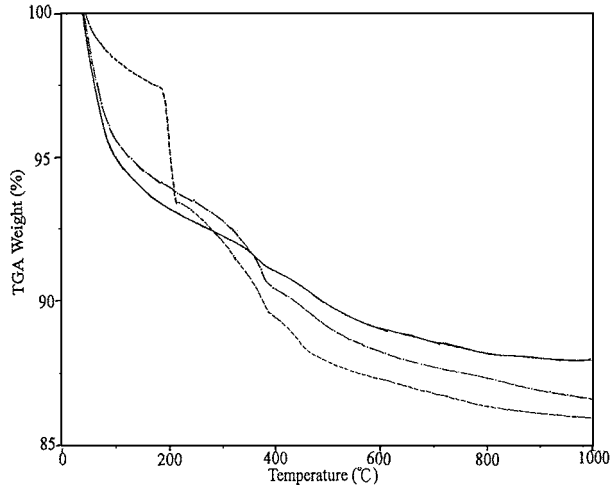

Figure 3 TGA results for H_2O-gel (solid line), Eth-gel (-.-.-), and Oct-gel (- - -).

H_2O-gel and Eth-gel. This peak corresponds to the vaporization of water from these two kinds of powders. Compared to H_2O-gel and Eth-gel, the DTA result for Oct-gel reveals no peak near 100°C. However, the DTA result for Oct-gel shows one remarkable exothermic peak starting at 190°C, which corresponds to the boiling of octanol.

The TGA measurements were carried out to determine the temperature range where solvent is released by the powders. As shown in Fig. 3, the TGA results for H_2O-gel, Eth-gel, and Oct-gel indicate that weight loss occurs in the range of 50 to 1000°C, with most of the water content being released between 50 to 200°C. The weight loss between 50 to 200°C for H_2O-gel and Eth-gel were about 7.1 and 6.4%, respectively. From this result, it seems that ethanol did not replace much water within the gel during the preparation process.

From the TGA results for Oct-gel, the weight loss between 50 to 200°C was much smaller than those for H_2O-gel and Eth-gel. However, it reveals a dramatic weight loss of about 4.5% at around 190°C. This shows that octanol is effective in replacing water within the gel.

From DTA and TGA results, it clearly shows that the high-carbon (long chain, high boiling point) alcohol of octanol is obviously more effective in replacing water in the gel than ethanol, which is used by the previous process of the sol-gel method.

3.2. Density result

Fig. 4 presents the relative densities of the compact disks from H_2O-powder, Eth-powder and Oct-powder calcined at different temperature in air. The three kinds of compact disks seem to have same relative density (∼81–82%) at the calcination temperature of 1000°C. At the calcination temperature of 1100°C, the relative density of Oct-powder becomes higher than those of H_2O-powder and Eth-powder. However, as the calcination temperature increased to 1200°C, the relative density of Oct-powder becomes 92% and is much higher than those of H_2O-powder and Eth-powder. This is very close to the density requirement (>94%) for electrolyte.

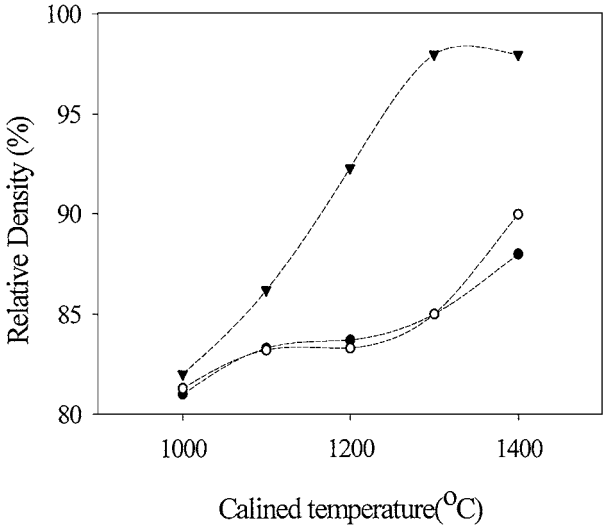

Figure 4 Density distribution of different powder compact disks after calcination of 5 hours at different temperature, (●) H_2O-powder, (○) Eth-powder, and (▼) Oct-powder.

Above 1300°C, the density of the compact disk of Oct-powder becomes fairly close to near-full relative density (about 98% to the theoretical density). This is the lowest calcination temperature as we know to synthesize doped ceria with high relative density.

From Fig. 4, it shows that Oct-powder shrinks very fast since its relative density increases from 82% to 98% within 300°C. This implies that the Oct-powders are soft-agglomerated. The soft-agglomerated powders pack uniformly, resulting in homogenous shrinkage of powder compacts to near-full density. Contrary to the density result of Oct-powder, H_2O-powder and Eth-powder seem to be more difficult to densify even after calcining at 1400°C for 5 hours. This implies that H_2O-powder and Eth-powder as prepared in this work consist of hard agglomerates. The hard agglomerates result in localized densification and leave a signification fraction of residual porosity.

3.3. X-ray analysis and crystallite size results

As shown in Fig. 5 for powders obtained from Oct-gel, initial crystallization into fluorite structure have taken place for Oct-gel after heating at 80°C for 5 hours, which is the lowest temperature for the fluorite structure formation at the best knowledge of us.

The XRD patterns obtained after heating the gels sequentially to higher temperatures are shown in Fig. 5. Heating the gels to 500°C has little effect on peak width and intensity, indicating little change in crystallite size. However, after heating at 1200°C, the peaks' widths become very narrow and intense, indicating rapid increase in the growth of the crystallite size.

The strongest peak of SDC was obtained at a scanning rate of 1°/min between $2\theta = 28°–35°$ in order to determine the precise width of the strongest peak at half maximum height. The crystallite sizes as measured by X-ray line broadening were estimated to be 4.7 nm for Oct-gel, compared to 5.6 nm for both H_2O-gel and Eth-gel. Results show that nanocrystalline gels were produced from three kinds of processes. However, the gel produced from the modified process composed of crystallite size that is 20% smaller than that prepared from the previous processes. This means that weaker interaction has been produced between crystallites by the modified process than that by the previous processes.

Theoretically, to achieve good sinterability, the ceramic powder should consist of particles with at least one of the following characteristics: good sinterable surface compositional gradients, small size, and soft agglomerates. Unfortunately, as shown above for H_2O-gel and Eth-gel, hard-agglomerated nanocrystalline particles were always produced which make sintering difficult. On the other hand, near-completely soft-agglomerated nanocrystalline particles can be produced from the modified process. From the crystallites size analysis and the sintering behavior as described above, it is implied that the soft agglomerate is the dominant factor that influences the sinterability.

3.4. Particle size analysis result

The particle size distribution is used to determine the agglomerating uniformity. From Fig. 6, it is seen that the agglomeration is between 200 and 2300 nm for H_2O-powder, between 500 and 2000 nm for Eth-powder,

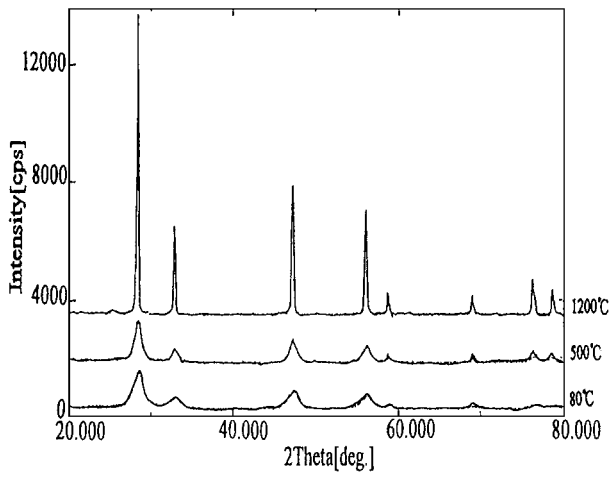

Figure 5 XRD results for Oct-gel at different calcination temperature.

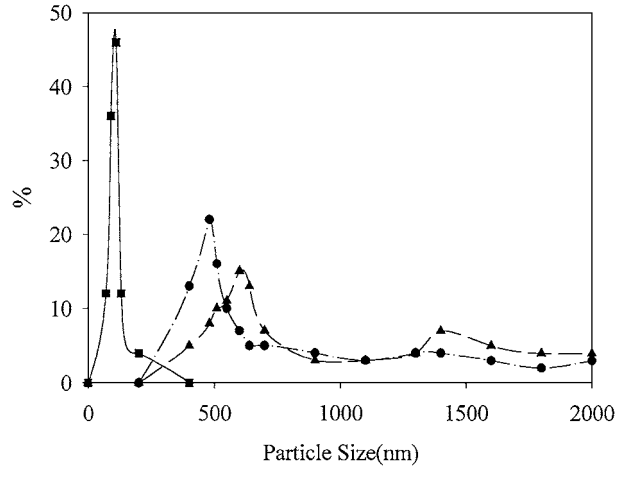

Figure 6 Particle size distribution of H_2O-powder (▲), Eth-powder (●), and Oct-Powder (■) calcined at 500°C.

and between 90 and 150 nm for Oct-powder. Hard agglomerates, which strengthen the binding at the contact points among crystallites, are formed during the drying and calcining steps. From the particle size distribution results, the powders from H_2O-gel and Eth-gel contain much more hard agglomerates than that from Oct-gel, which has good uniformity.

The particle size distribution will affect densification and thus the density after calcination. During ball milling, the hard agglomerates in H_2O-powder and Eth-powder can not be completely broken down to produce uniform powders. As the densification starts, the densely packed regions densify first, pull away from the surrounding regions, and thus leave large pores, which inhibit complete densification during calcination. However, the near-completely soft-agglomerated Oct-powder can be almost completely broken down during ball milling and consequently does not impede densification.

3.5. Mechanism of agglomeration

3.5.1. Hard agglomerates in H_2O-gel

The formation of the hard agglomerates may be explained by the surface chemistry argument [16]. For H_2O-gel, hydrous oxide particles (SDC-$x$$H_2O$) are surrounded by molecular H_2O. In cases where powder particles are in close contact, particle bridging by hydrogen bonding of water to two terminal hydroxyl groups occurs as shown in Fig. 7a. As the drying of the powders commences, the "bridging" water molecules released from the crystallite and the crystallites are close enough that hydrogen bonding occurs between two terminal hydroxyl groups of different particles as shown in Fig. 7b. Because of the close proximity of the hydrogen-bond hydroxyl groups, further dehydration leads to the formation of actual chemical bonds preferentially between particles as shown in Fig. 7c. This yields hard agglomerates.

This mechanism of hard-agglomerate formation is supported by the result of the crystallites size of dry H_2O-gel (5.6 nm), compared to that of Oct-gel (4.7 nm), and also by the non-uniform particle size distribution of H_2O-powder. In addition, low density is expected for H_2O-powder even at high calcination temperature of 1400°C. These results are consistent with those of Rodes [17] and Lange [18], who demonstrated that non-uniform packing from hard agglomerates can lead to localized and inhomogeneous densification.

By washing the gel with ethanol, the hydrous particles should be surrounded by ethanol. The strong bonding between hydrous particles should be replaced with Van der Waal force and thus soft agglomerates are formed [15]. However, in this work, some hard agglomerates still remain in Eth-gel, as shown by the particle size distribution and density results. This may be due to the low boiling point and high missibility of ethanol with water, which make the complete replacement of water by ethanol is not easy during the washing and drying stages. One may use more ethanol with more times than that employed in the work to achieve higher replacement of water by ethanol. Therefore, in this work, the molecule water in the gel could not be completely replaced by ethanol and some hydrogen bonding within Eth-gel remains and results in some hard agglomerates.

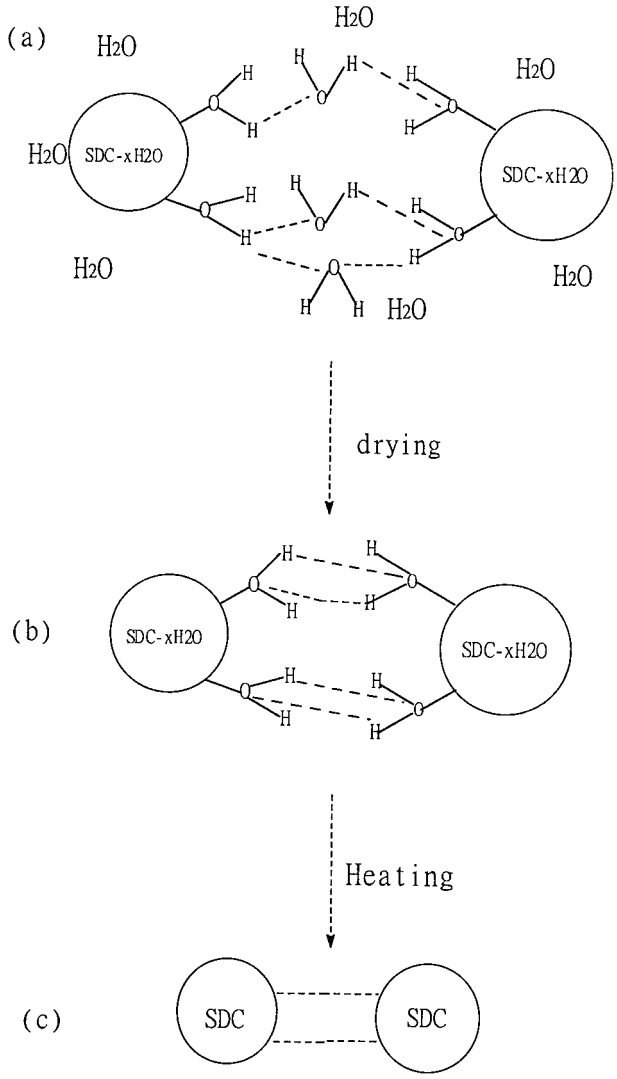

Figure 7 Proposed mechanism for hard agglomerate formation in H_2O-gel.

3.5.2. Soft agglomerates in Oct-gel

In the modified process, the replacement of water with octanol by gently heating the gel in octanol provides the basis for agglomeration control. As drying commences, the long-chain alcohol replaces the "bridging" water, as shown in Fig. 8a to b. The long-chain alcohol between the particles acts to prevent the close approach of the particles due to a steric effect; thus, as the drying temperature increases, continued removal of the molecule water in the gel will not result in close approach of the particles, as shown in Fig. 8c. This is the key of the modified process to form soft agglomerates. Therefore, separated crystallites form without interaction, as shown in Fig. 8d. This is why the crystallite size of the soft-agglomerated Oct-gel is smaller than that of the hard-agglomerated H_2O-gel.

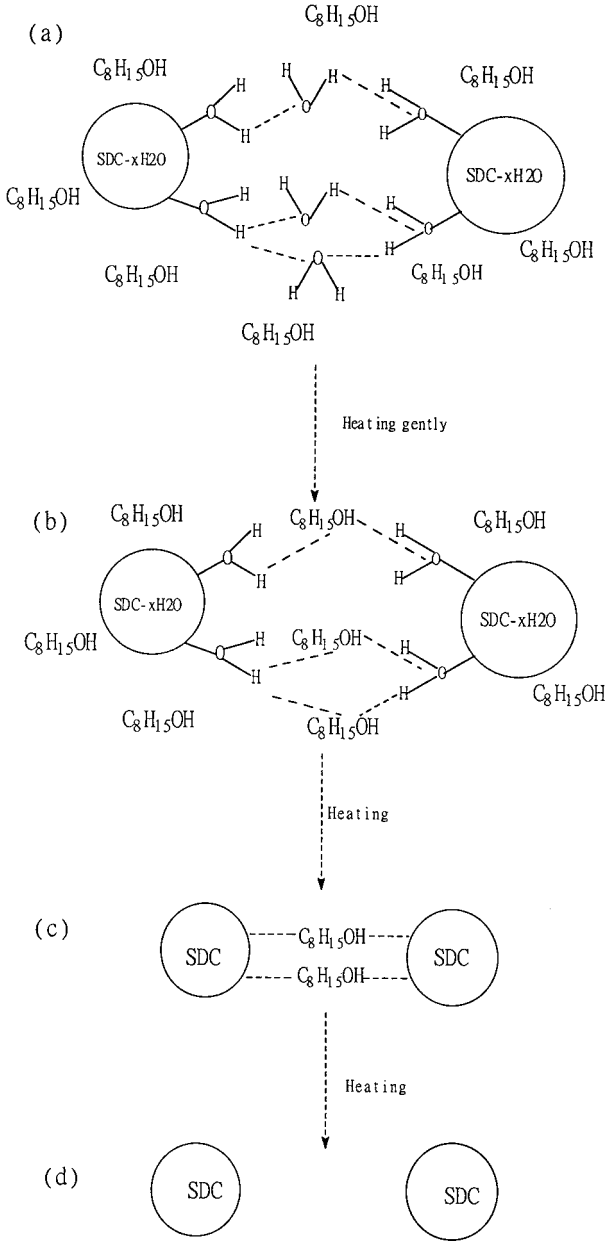

Figure 8 Proposed mechanism for soft agglomerate formation in Oct-gel.

4. Conclusion

Three kinds of gels made from different processes have been used to produce SDC powders. Although all processes can form nanocrystalline powder, the results of the crystallite size and the particle size distribution show that the agglomerate strength is the dominant factor for the final sintering density. The gels prepared from the previous processes (H_2O-gel and Eth-gel) consist of hard agglomerates. Only 90% relative density was achieved even when sintering was carried out at 1400°C for 5 hours. However, the gel prepared in the modified process can be sintered to a higher relative density even at relatively low sintering temperature of 1300°C. This is because the modified process involves treating the gel with octanol, which may prevent interaction between particles. Thus, the possibility of any chemical bonds forming between particles during drying is significantly reduced. This inhibits the formation of hard agglomerates and thus near-completely soft agglomerates are formed which leads to near-fully relative density after sintering.

References

1. B. RILEY, *J. Power Sources* **29** (1990) 223.
2. K. EGUCHI, T. SETOGUCHI, T. INOUE and H. ARAI, *Solid State Ionics* **52** (1992) 165.
3. H. YAHIRO, Y. BABA, K. EGUCHI and H. ARAI, *J. Electrochem. Soc.* **135** (1988) 2077.
4. K. R. THAMPI, A. J. MCEOVY and J. VANHERLE, *Ibid.* **142** (1993) 506.
5. C. C. CHEN, M. M. NASRALLAH and H. U. ANDERSON, *ibid.* **140** (1983) 3555.
6. E. J. L. SCHOULER and M. KLEITZ, *ibid.* **134** (1987) 1045.
7. H. L. TULLER, *Solid State Ionics* **52** (1992) 165.
8. I. REISS, D. BRAUNSHTEIN and D. S. TANNHAUSER, *J. Amer. Ceram. Soc.* **64** (1981) 479.
9. T. KUDO and H. OBAYASHI, *J. Electrochem. Soc.* **122** (1975) 142.
10. Y. S. ZHEN, S. J. MILNE and R. J. BROOK, *Sci. Ceram.* **14** (1988) 1025.
11. K. Q. HUANG, M. FENG and J. B. GOODENOUGH, *J. Amer. Ceram. Soc.* **81**(2) (1998) 357.
12. J. V. HERLE, T. HORITA, T. KAWADA, N. SAKAI, H. YOKOKAWA and M. DOKIYA, *Solid State Ionics* **86–88** (1996) 1255.
13. W. HUANG, P. SHUK and M. GREENBLATT, *ibid.* **100** (1997) 23.
14. S. DIKMEN, P. SHUK and M. GREENBLATT, *ibid.* **126** (1999) 89.
15. M. J. READEY, R. R. LEE, J. W. HALLORAN and A. H. HEUER, *J. Amer. Ceram. Soc.* **73**(6) (1990) 1499.
16. M. S. KALISZEWSKI and A. H. HEUER, *ibid.* **73**(6) (1990) 1504.
17. W. H. RHODES, *ibid.* **64**(1) (1981) 19.
18. F. F. LANGE, *ibid.* **76**(2) (1984) 83.

Received 11 October 2000
and accepted 13 August 2001